ACS APPLIED MATERIALS & INTERFACES

Research Article

www.acsami.org

One-Pot Environmentally Friendly Approach toward Highly Catalytically Active Bimetal-Nanoparticle-Graphene Hybrids

Chang-Hai Liu,[†,‡] Xiao-Qi Chen,[§] Yong-Feng Hu,[†,§] Tsun-Kong Sham,[†,§,⊥] Qi-Jun Sun,[†,‡] Jian-Bing Chang,[†,‡] Xu Gao,[†,‡] Xu-Hui Sun,[†,‡] and Sui-Dong Wang*[,†,‡]

[†]Soochow University-Western University Joint Centre for Synchrotron Radiation Research, and [‡]Jiangsu Key Laboratory for Carbon-based Functional Materials & Devices, Institute of Functional Nano & Soft Materials (FUNSOM), Soochow University, Suzhou, Jiangsu 215123, P. R. China

[§]Canadian Light Source, University of Saskatchewan, Saskatoon, Saskatchewan S7N 0X4, Canada

[⊥]Department of Chemistry, University of Western Ontario, London, Ontario N6A 5B7, Canada

Supporting Information

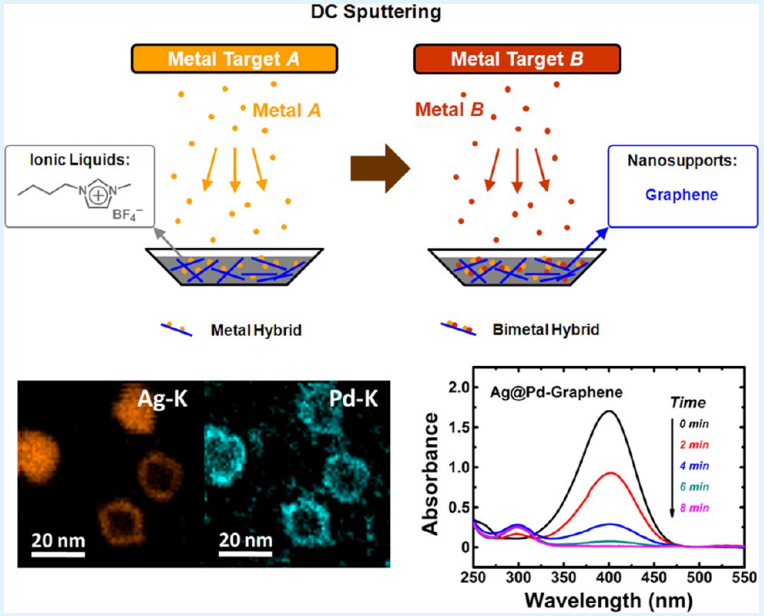

ABSTRACT: A one-pot universal approach with simple metal sputtering onto room temperature ionic liquids has been developed to prepare bimetal-nanoparticle (NP)-graphene hybrids, and the process is environmentally friendly and completely free of additives and byproducts. The graphene-supported bimetallic NPs have an Ag-based core and an Au/Pd-rich shell, demonstrated by the scanning transmission electron microscopy. The X-ray absorption near-edge spectroscopy using synchrotron radiation reveals the occurrence of charge redistribution at both the Ag@Au and Ag@Pd core−shell interfaces. The as-prepared Ag@Au and Ag@Pd bimetal-NP-graphene hybrids are highly catalytically active for reduction of 4-nitrophenol, whose catalytic activity is superior to the corresponding monometallic hybrids. The catalytic superiority is ascribed to the electronic structure modification and morphological irregularity of the graphene-supported bimetallic NPs.

KEYWORDS: *bimetal nanoparticles, graphene, hybrid, room temperature ionic liquids, sputtering*

1. INTRODUCTION

Bimetallic nanoparticles (NPs), composed of two chemically distinct metals with core-shell, intermixed or alloyed nanostructures, have aroused extensive interests because of their unique optical, electronic, magnetic, and especially catalytic properties.[1−4] The bimetallic-NP-based catalysts often show superior catalytic activity compared with the homologous monometallic counterparts, arising from the synergistic effects of both moieties.[4−9] To prevent bimetallic NPs from aggregation and coalescence which reduces the catalytic activity and surface area, appropriate supports immobilizing bimetallic NPs are widely utilized. As a remarkable nanosupport, graphene possesses huge surface area, high conductivity, and rich physical and chemical functionalities by surface modification.[10−12]

Received: March 11, 2013
Accepted: May 13, 2013
Published: May 13, 2013

   dx.doi.org/10.1021/am4008853 | ACS Appl. Mater. Interfaces 2013, 5, 5072−5079

Scheme 1. Scheme of Preparation Method for Bimetal-NP-Graphene Hybrids: Sputtering Metal *A* Followed by Sputtering Metal *B* onto RTILs, in Which Graphene Is Predispersed[a]

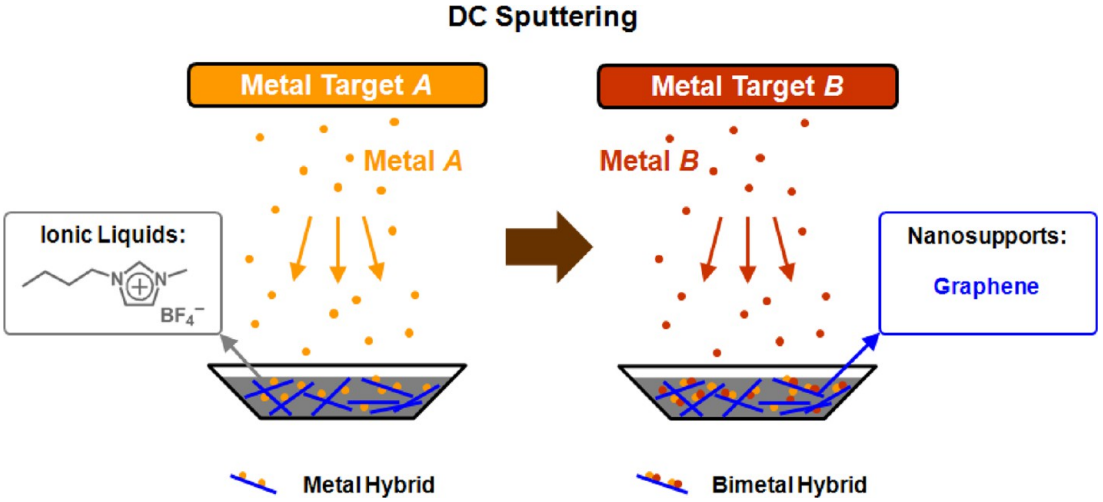

[a]There are neither additives nor byproducts in this simple process.

Numerous studies have been conducted on graphene-supported metal NPs,[13,14] including Au,[15,16] Ag,[17] Pd,[18,19] Pt monometallic NPs,[20,21] and bimetallic NPs,[22−24] which show great potential for diverse applications in catalysis, energy and sensing. As graphene could not only stabilize bimetallic NPs but also facilitate mass transport in catalytic reaction process, the incorporation of bimetallic NPs with graphene as a composite is an effective strategy to prepare highly catalytically active nano-sized hybrids.

Conventional synthesis of bimetallic NP hybrids typically involves simultaneous or successive chemical reduction of two different metal precursors,[1−4,22−24] which often requires employment of reducing or stabilizing agents, and byproducts are often produced. Towards an additive and byproduct free approach, we have recently developed an alternative strategy with easy processing to prepare the metal-NP-carbon-nanostructure hybrids.[25] This method utilizes simple metal sputtering onto room temperature ionic liquids (RTILs),[26,27] in which small-sized metal NPs can form spontaneously and self assemble on pre-dispersed carbon nanostructures.[25] The one-pot process is completely free of additives and byproducts, and RTILs are recyclable and green-chemistry compatible. It is thus environmentally friendly with high flexibility and controllability. In the present report, the method is further developed, for the first time, to prepare the bimetal-NP-graphene hybrids such as the Ag@Pd and Ag@Au ones with bimetallic core-shell-like structure. The bimetallic nanohybrids exhibit excellent catalytic activity for reduction of 4-nitrophenol, which is far superior to those of the monometallic counterparts. The advanced microscopic and spectroscopic characterizations demonstrate the formation of a bimetallic core−shell-like structure and consequent crystalline and electronic structure modifications, which are considered to induce the prominent synergistic effects for catalytic applications.

The preparation procedure of the bimetal-NP-graphene hybrids is depicted in Scheme 1. The commercially available graphene is firstly dispersed in a RTIL, l-butyl-3-methylimidazolium tetrafluoroborate ([BMIm][BF_4]) to form the graphene-RTIL suspension. Subsequently, Ag is directly sputtered onto the suspension, followed by the Au or Pd sputtering with a simple switch of the metal target. The corresponding Ag@Pd or Ag@Au bimetal-NP-graphene hybrids are spontaneously formed in the RTIL, and the composition and proportion of the bimetallic NPs could be easily controlled by changing the metal targets and sputtering parameters. Note that the graphene sheets play a key role not only as the nanosupport with a huge surface area, but also as the stabilizer to anchor the catalytically active bimetallic NPs. In the absence of graphene, the bimetallic NPs tend to aggregate upon the washing process for removing the RTIL. In addition, the RTIL is necessary for the hybrid preparation: (1) The metal NPs may nucleate on the RTIL surface and then diffuse into the RTIL,[28] and thus full dispersion of graphene in the RTIL is needed for uniform decoration of the metal NPs. (2) The RTIL could act as a linker to anchor the metal NPs on graphene.[25,29] (3) The RTIL enables sputtering onto liquid under high-vacuum circumstance due to its extremely low vapor pressure.[26,27]

2. EXPERIMENTAL SECTION

2.1. Preparation of Bimetal-NP-Graphene Hybrids. As depicted in Scheme 1, the bimetal-NP-graphene hybrids were prepared by successive sputtering of the metal of interest onto the graphene-RTIL suspension. First, 2 mg of graphene powder was fully dispersed into 1 ml [BMIm][BF_4] with ultrasonication for 10 min. Second, the black graphene-RTIL suspension was placed into a clean stainless steel pot, and Ag was sputtered onto the graphene-RTIL suspension at room temperature for 120 s in a desktop direct-current sputtering system (Quorum Technologies, equipped with a thickness monitor which is calibrated by a surface profiler). The Ar working pressure and deposition rate were kept at about 0.01 mbar and 0.2 Å/s, respectively. Third, Au or Pd was sputtered onto the Ag-graphene-RTIL suspension under identical sputtering conditions by simply altering the metal target. Note that the total sputtered metal thickness is controlled to be same for all the hybrids, e.g., 2.4 nm Ag plus 2.4 nm Pd for the Ag@Pd bimetallic hybrid, and correspondingly 4.8 nm Pd for the monometallic Pd hybrid. The control of the metal content is necessary for a reliable comparison in catalytic activity of the different hybrids. Eventually, the bimetal-NP-graphene hybrids were separated from [BMIm][BF_4] with high-speed centrifugation and decantation, followed by washing in an ultrasonic bath of acetone. This cleaning process was repeated several times to completely remove residual [BMIm][BF_4] from the bimetal-NP-graphene hybrids (in dry powder form). The estimated loadings of the Ag@Au and Ag@Pd bimetallic

dx.doi.org/10.1021/am4008853 | ACS Appl. Mater. Interfaces 2013, 5, 5072−5079

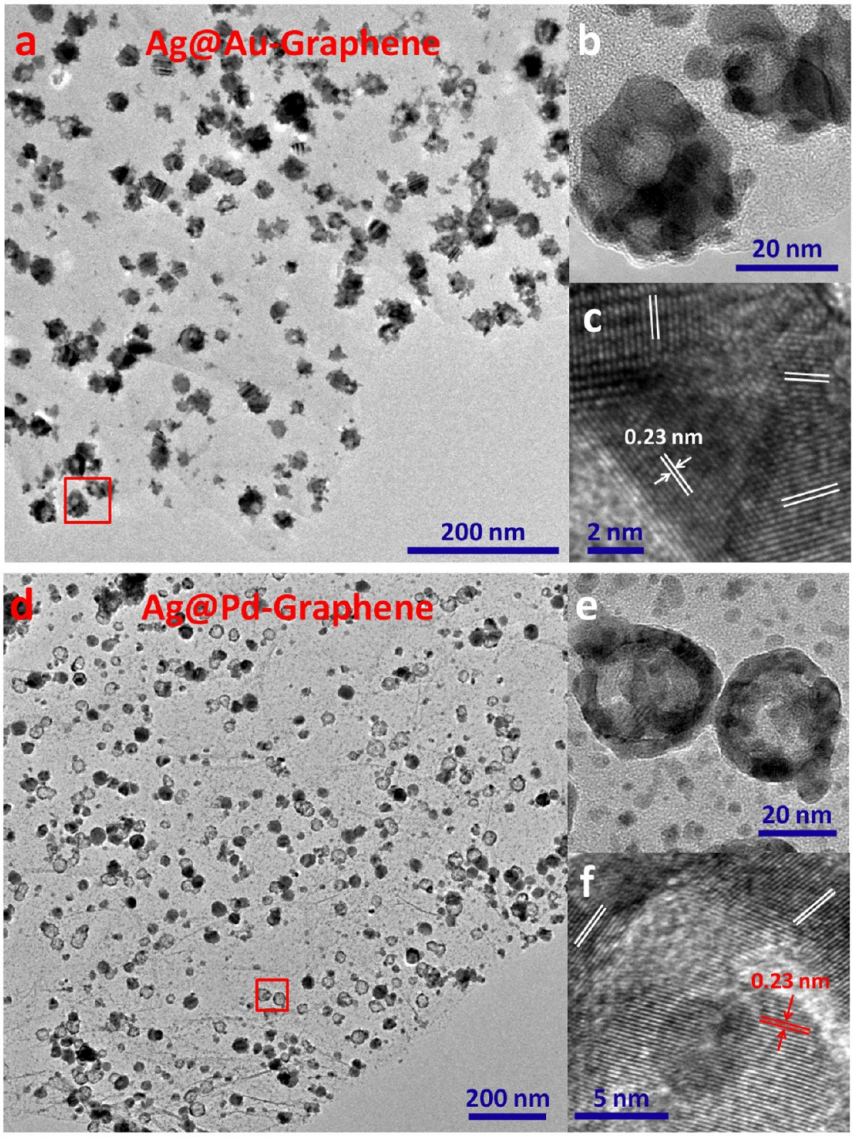

Figure 1. (a, b) TEM and (c) HRTEM images of Ag@Au bimetal-NP-graphene hybrid, where b is magnified small square shown in a. (d, e) TEM and (f) HRTEM images of Ag@Pd bimetal-NP-graphene hybrid, where e is magnified small square shown in d.

NPs on graphene (by thermogravimetric analysis) are about 13.1 wt % and 10.6 wt %, respectively.

[BMIm][BF_4] (purity >99%) was purchased from Shanghai Cheng-Jie Chemical and purified in vacuum for 24 h before using. Graphene powder was purchased from Nanjing XFNANO Materials Tech, prepared by thermal exfoliation reduction and hydrogen reduction. 4-Nitrophenol and $NaBH_4$ were purchased from Aldrich and used as received.

2.2. Characterization of Bimetal-NP-Graphene Hybrids. The microscopic structures of the bimetal-NP-graphene hybrids were characterized with the high-resolution transmission electron microscopy (HRTEM, FEI Quanta FRG 200F, operating at 200 kV) and the high-angle annular dark-field scanning TEM (HAADF-STEM). The crystalline structures of the bimetal-NP-graphene hybrids were characterized with the X-ray diffraction (XRD, PANalytical, Empyrean). The electronic structures of the bimetal-NP-graphene hybrids were characterized with the X-ray photoemission spectroscopy (XPS, Kratos Axis Ultra DLD, monochromatic Al $K\alpha$) in ultrahigh vacuum. The Pd and Au L-edge X-ray absorption near-edge structure (XANES) measurements were carried out at the SXRMB beamline of the Canadian Light Source (CLS) and the BL14W1 beamline of the Shanghai Synchrotron Radiation Facility (SSRF), respectively. The time-dependent UV−vis measurements were carried out with a UV-vis-NIR spectrophotometer (PerkinElmer, Lambda 750).

2.3. Catalytic Reaction with Bimetal-NP-Graphene Hybrids. The reaction rate of the 4-nitrophenol reduction was evaluated by the UV−vis absorption spectroscopy with 2 min measuring intervals, where the scanning range was from 250 nm to 550 nm and the data were recorded at room temperature without stirring. 0.1 mg metal-NP-graphene hybrids or bimetal-NP-graphene hybrids were added into a quartz cuvette containing 2 mL aqueous solution of $NaBH_4$ (5 mM/L) to get a mixed solution. Afterwards, 1 mL of 4-nitrophenol aqueous solution (0.2 mM/L) was added into the mixed solution for the absorption measurements. Purified deionized water was used as the reference.

3. RESULTS AND DISCUSSION

3.1. Characterization of Bimetal-NP-Graphene Hybrids. The TEM and HRTEM images of the bimetal-NP-graphene hybrids are shown in Figure1, where the bimetallic NPs are randomly decorated on graphene with the flower-like or doughnut-like morphology. The morphology is distinct from the circular NP shape in the monometal-NP-graphene

dx.doi.org/10.1021/am4008853 | ACS Appl. Mater. Interfaces 2013, 5, 5072−5079

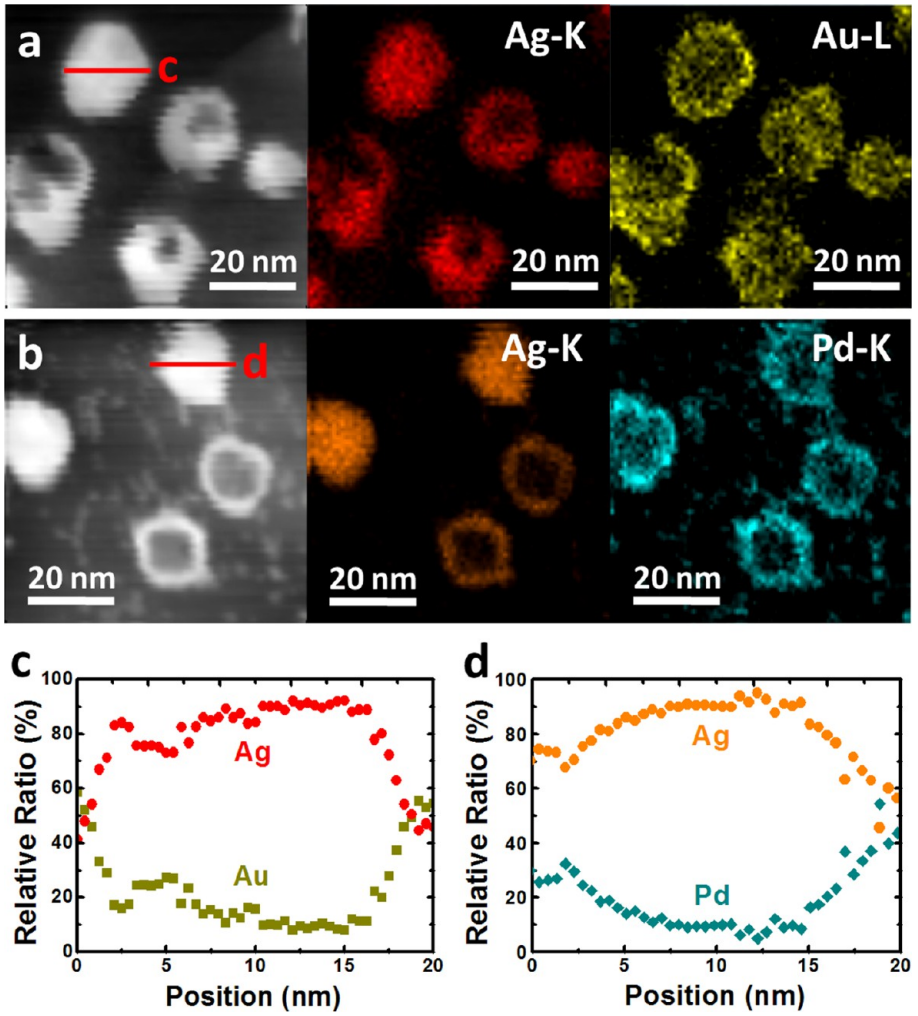

Figure 2. (a) HAADF-STEM images of Ag@Au bimetal-NP-graphene hybrid, where elemental mapping of Ag and Au are separately shown. (b) HAADF-STEM images of Ag@Pd bimetal-NP-graphene hybrid, where elemental mapping of Ag and Pd are separately shown. Crossline profiles of elemental composition for (c) Ag@Au and (d) Ag@Pd bimetallic NPs shown in a and b, respectively. The crossline length in a and b is 20 nm.

hybrids,[25] and the TEM and HRTEM images of the Ag-NP-graphene, Au-NP-graphene and Pd-NP-graphene hybrids are shown in Figure S1, S2, and S3 (see the Supplementary Information) as references, respectively. Figure1a−1c correspond to the Ag@Au hybrid, which shows that the Ag@Au NPs exhibit the inhomogeneous morphology, typically with a lighter core coated by a darker shell due to the elemental contrast and/or thickness variance. According to the sputtering sequence of Ag followed by Au, the bimetallic "core−shell-like" structure (generically defined, see below) is considered to consist of an Ag-based core and an Au-rich shell. As the Au NPs (several nm) prepared by the present method are smaller than the Ag NPs (10−20 nm) on carbon nanostructures,[25] the Au-rich shell is composed of multiple small-sized Au NPs (Figure1b). As demonstrated by the HRTEM image shown in Figure1c, different growth directions are present within an Ag@Au core-shell-like structure, all of which have an identical interplanar spacing of 2.3 Å in accord with the (111) lattice planes of face-centered cubic (fcc) Ag and Au. Similar bimetallic NP morphology was observed for the Ag@Pd hybrid, with the co-occurrence of some small-sized Pd monometallic NPs (several nm) among the bimetallic NPs, as shown in Figure 1d−f. Furthermore, a doughnut-like structure appears as well in the Ag@Pd case (Figure1d), and the formation mechanism for this particular structure is unclear yet.

To verify the bimetallic core−shell-like structure, the HAADF-STEM was utilized to map the elemental spatial distribution. Figure 2a, b show the STEM mapping for the Ag@Au and Ag@Pd bimetallic NPs, respectively, and it is clear that the core of the bimetallic NPs is Ag-based and the shell is Au-rich or Pd-rich. The crossline profiles of the elemental composition for the Ag@Au and Ag@Pd bimetallic NPs are shown in Figure 2c, d, respectively. There is coexistence of both metal moieties in the shell region, suggesting that local alloying via metal interdiffusion at the core-shell interface has taken place. Considering that the different metal sputtering is successive, the Ag-NP-graphene hybrid is formed first in the RTIL, and subsequently the Au/Pd NPs are attached to the Ag NPs on graphene. The formation of the core−shell-like bimetallic structure may be driven by the thermodynamic forces, e.g., by the spontaneous exothermic interaction between Ag and Au/Pd.[30] The core−shell-like morphology is expected to have a great impact on the crystalline and electronic structures of the bimetallic NPs, which are discussed below.

The XRD patterns of the bimetal-NP-graphene hybrids and the corresponding monometal-NP-graphene hybrids are shown in Figure3, where the features at 2θ of about 38, 44, 64, and 78°

dx.doi.org/10.1021/am4008853 | ACS Appl. Mater. Interfaces 2013, 5, 5072−5079

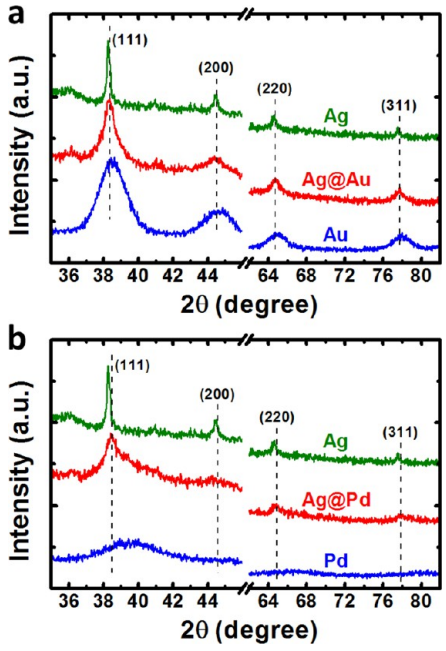

Figure 3. (a) XRD patterns of Ag@Au bimetal-NP-graphene hybrid, and of Ag and Au monometal-NP-graphene hybrids. (b) XRD patterns of Ag@Pd bimetal-NP-graphene hybrid, and of Ag and Pd monometal-NP-graphene hybrids.

can be assigned to the fcc lattice planes of (111), (200), (220), and (311),[2,3] respectively. In the case of the Ag@Au hybrid (Figure3a), all the diffraction peaks are in between the corresponding peaks of the Ag and Au monometallic hybrids. These intermediate peak positions indicate the occurrence of the crystalline structure modification attributable to the local alloying at the Ag@Au core−shell interface. The similar characteristics are present for the Ag@Pd hybrid (Figure3b), where the peak shift is more prominent due to a larger 2θ difference between the Ag and Pd diffraction patterns. Note that the diffraction peaks of the Au and Pd hybrids are much broader compared with those of the Ag hybrid, owing to the fact that the Au and Pd NPs are smaller than the Ag NPs (Figures S1, S2, and S3 in theSupporting Information).[25]

The XANES using synchrotron radiation is an advanced technique to probe the electronic structure modification of bimetallic systems,[31−36] often involving the d-band charge redistribution which could be critical to their catalytic activity.[4] The Pd L_3-edge (dipole transition from 2p to 4d, carried out at the SXRMB beamline of CLS) XANES spectra are shown in Figure4a, in which the intense absorption peak at the edge jump known as the whiteline probes the density of unoccupied states in the d-band (d-holes).[31−36] Because the d-band of Pd extends above the Fermi Level (the d-band is not fully filled) and has high and narrow density of unoccupied states, the whiteline at about 3175 eV is intense as shown in Figure4a. Compared with the Pd bulk, the whiteline of the Pd-NP-graphene hybrid is shifted to a higher energy and becomes more intense due to the large surface area and surface oxidation of the Pd NPs, resulting in more d-holes (Pd losing *d* electrons). This observation is supported by the XPS Pd 3*d* spectra shown in FigureS4a (see the Supporting Information), where the Pd oxidation feature appears on the higher binding energy side. Significantly, upon the formation of the Ag@Pd bimetallic NPs, the whiteline intensity of the Ag@Pd hybrid is

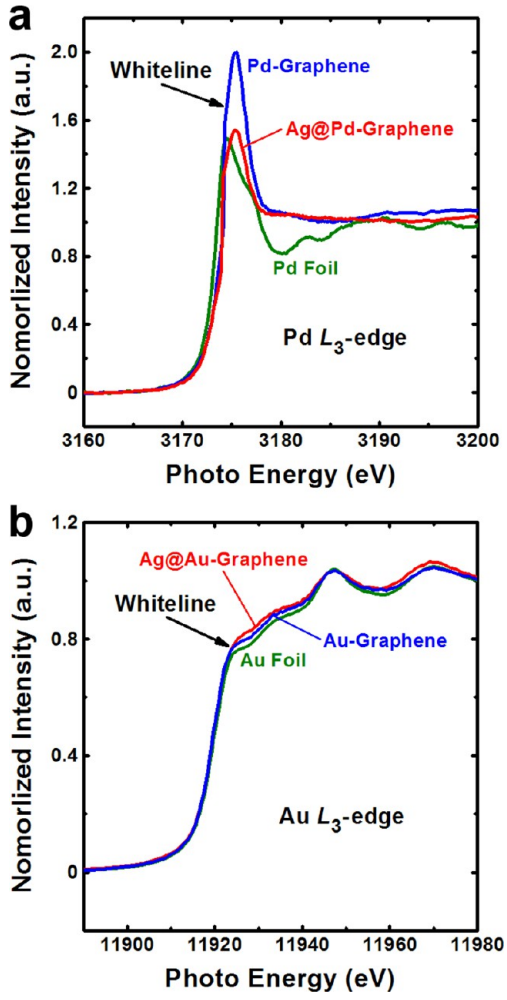

Figure 4. (a) Synchrotron radiation XANES Pd L_3-edge spectra of Ag@Pd bimetal-NP-graphene hybrid, of Pd monometal-NP-graphene hybrid and of Pd bulk. (b) Synchrotron radiation XANES Au L_3-edge spectra of Ag@Au bimetal-NP-graphene hybrid, of Au monometal-NP-graphene hybrid and of Au bulk.

greatly reduced as shown in Figure4a, indicating that the Pd d-band gains electrons from Ag.[35,36] This charge redistribution is supported by the emergence of the feature on the lower binding energy side (increasing d screening) in the XPS Pd 3d spectra (see FigureS4a in the Supporting Information),[37] and it is in excellent agreement with the previous report on the Ag@Pd alloys.[31]

We now turn to the Au results. The Au L_3-edge (dipole transition from 2p to 5d, carried out at the BL14W1 beamline of SSRF) XANES spectra are shown in Figure4b, in which the whiteline is not intense as the *d*-band of Au is nominally full and lies below the Fermi level, although some Au 5d character is present above the Fermi level via hybridization with the conduction electrons. For the Ag@Au hybrid, the whiteline intensity is increased compared with the Au-NP-graphene hybrid and Au bulk, as demonstrated in Figure4b. It indicates the depletion of Au d-band electrons due to electron transfer to Ag, in good agreement with the XPS Au 4f spectra (FigureS4b in Supplementary Information) in which the feature on the higher binding energy side is enhanced with the Ag promotion.[38] The XANES results demonstrate strong interaction of both metal moieties in the bimetal-NP-graphene hybrids, which induces local alloying at the core−shell interface.

dx.doi.org/10.1021/am4008853 | ACS Appl. Mater. Interfaces 2013, 5, 5072−5079

3.2. Catalytic Performance of Bimetal-NP-Graphene Hybrids. According to the crystalline and electronic structure modifications in the bimetal-NP-graphene hybrids, some synergistic effects for catalytic applications could be expected. A typical catalysis reaction, e.g., reduction reaction of 4-nitrophenol into 4-aminophenol with a large excess of $NaBH_4$,[5,8,9,39,40] is selected to evaluate the catalytic activity of the bimetal-NP-graphene hybrids. Upon mixing $NaBH_4$ with 4-nitrophenol in aqueous solution, the UV−vis absorption spectrum is dominated by a characteristic absorption peak at about 400 nm due to the nitro compound.[5,8,9,39,40] With the addition of pristine graphene, there is no evidence of reduction (see Figure S5a in the Supplementary Information) within the measuring time scale. In the case of the addition of the Ag-NP-graphene hybrid, the reduction reaction is quite slow (see Figure S5b in the Supporting Information), indicating the low catalytic activity of the Ag-NP-graphene hybrid presumably due to the relatively large size and surface oxidation of the Ag NPs.[9] We can exclude the pristine graphene and Ag-NP-graphene hybrid as the active catalysts based on these observations. However, the reduction reaction occurs immediately with the addition of the bimetal-NP-graphene hybrids, as monitored by the time-dependent UV-vis absorption spectroscopy shown in panels a and b in Figure 5 for the Ag@Pd and Ag@Au hybrids, respectively. It is evident from these spectra that the characteristic peak at about 400 nm arising from 4-nitrophenol decreases rapidly, accompanied by the increase of a new peak at about 300 nm arising from 4-aminophenol,[5,8,9,39,40] the reduction product of 4-nitrophenol. The eventual disappearance of the 400 nm peak in panels a and b in Figure 5 indicates the complete reduction of 4-nitrophenol, demonstrating that the bimetal-NP-graphene hybrids are highly catalytically active. Significantly, the reduction reaction rates with the bimetal-NP-graphene hybrids are faster than those with the corresponding monometal-NP-graphene hybrids (Figure S5c and S5d in Supporting Information corresponding to the Pd and Au hybrids, respectively). Note that the total sputtered metal thickness is controlled to be same for all the hybrids, so the Au/Pd content for the bimetallic hybrids is less than the corresponding monometallic one.

To quantitatively evaluate the reaction kinetics, the plots of $\ln(A_t/A_0)$ vs the reaction time (t) for both the bimetal-NP-graphene and monometal-NP-graphene hybrids are shown in Figure5c, where A_t and A_0 are the time-dependent and initial ($t = 0$) absorbance of the 400-nm peak, respectively. The reaction rate constant (k) can be calculated from the slope of the linear fit of $\ln(A_t/A_0)$ vs t,[5,39] and accordingly the catalytic activity factor (k) is obtained by $k = k/m$ where m is the weight of the catalyst.[8,40] The k for the Ag@Pd bimetallic hybrid is as high as 86.7 s^{-1} g^{-1}, which is higher than 48.8 s^{-1} g^{-1} for the Pd monometallic hybrid; the k for the Ag@Au bimetallic hybrid is 53.6 s^{-1} g^{-1}, which is higher than 28.5 s^{-1} g^{-1} for the Au monometallic hybrid as well. The k values of the bimetallic hybrids for 4-nitrophenol reduction are among the best ones reported recently in the literature.[5,8,39,40] It is significant that the bimetal-NP-graphene hybrids possess higher catalytic activity than the monometallic counterparts, implying that the synergistic effects are at work due to the bimetallic incorporation.

On the basis of the above discussion, we propose that the underlying mechanism for the high catalytic activity of the bimetal-NP-graphene hybrids involves the following synergistic aspects: (1) The charge redistribution (Figure4) in the bimetallic NPs modifies the density of d-band electrons, which could enhance the catalytic activity and stability of one or both metal NP moieties.[4,41] Further studies such as the in situ XANES probing during catalytic process are needed to elucidate this electronic promoting effect. (2) The morphological irregularity (Figure1) of the bimetallic NPs induces more bimetallic interfaces and low-coordination-number edges/corners, which could behave as the catalytically active sites.[1,2] As the bimetallic NPs are apparently larger than the Au and Pd monometallic NPs, the NP size effect should not be the dominant effect in the present case. (3) The graphene nanosupport has enormous surface area and high conductivity,[10−12] which could benefit the reactant adsorption and electron transfer. The interaction mechanism between graphene and the metal NPs is still an open issue, and the possible stabilization mechanisms may include the electrostatic attraction arising from partial electron transfer between graphene and the metal NPs, and the proposed "nano-glue" effect by sandwiching RTIL monolayer between graphene and the metal NPs.[25,29] Overall speaking, it appears that the combination of the advanced microscopic and spectroscopic characterization (especially synchrotron radiation based char-

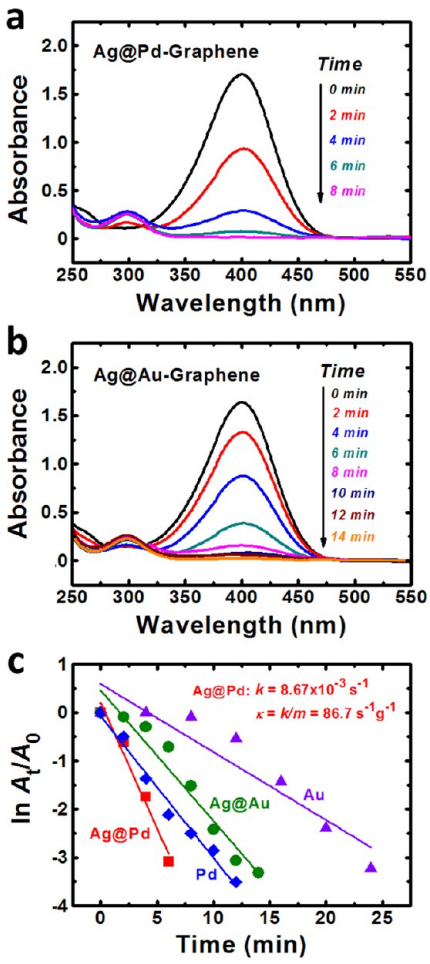

Figure 5. Time-dependent UV−vis absorption spectra for reduction of 4-nitrophenol using (a) Ag@Pd or (b) Ag@Au bimetal-NP-graphene hybrid as the catalyst. (c) Normalized absorption intensity of 4-nitrophenol $\ln(A_t/A_0)$ vs reaction time using Ag@Pd or Ag@Au bimetal-NP-graphene hybrid as the catalyst, where corresponding data with Pd or Au monometal-NP-graphene hybrid are shown for comparison.

dx.doi.org/10.1021/am4008853 | ACS Appl. Mater. Interfaces 2013, 5, 5072−5079

acterization) is a promising strategy to probe catalytically active nanosized hybrids.

4. CONCLUSIONS

The Ag@Au and Ag@Pd bimetal-NP-graphene hybrids can be prepared by simply conducting successive metal sputtering onto the graphene-RTIL suspension, and the bimetallic NPs have the core-shell-like structure with an Ag core and an Au/Pd shell. The graphene-supported bimetallic NPs show modified crystalline and electronic structures compared with the monometallic counterparts, which almost certainly arise from the local alloying at the core-shell interface. The bimetallic hybrids possess high catalytic activity for reduction of 4-nitrophenol with k up to 86.7 s^{-1} g^{-1}, which is higher than that of the corresponding Au or Pd monometallic hybrids. The catalytic superiority of the bimetallic hybrids is attributed to the synergistic effects arising from the favorable electronic and morphological modifications. It is worth emphasizing that the one-pot approach utilizes green-chemistry compatible RTILs and is completely free of additives and byproducts. Thus it is simple, clean, and environmentally friendly. The bimetal-NP-graphene hybrids are expected to have great potential in catalytic and sensing applications.

■ ASSOCIATED CONTENT

Supporting Information

TEM and HRTEM images of Ag, Au, and Pd monometal-NP-graphene hybrids; XPS spectra of Ag@Pd and Ag@Au bimetal-NP-graphene hybrids; UV-vis spectra for reduction of 4-nitrophenol with pristine graphene, and with Ag, Pd ,or Au monometal-NP-graphene hybrid. This material is available free of charge via the Internet at http://pubs.acs.org/.

■ AUTHOR INFORMATION

Corresponding Author

*E-mail: wangsd@suda.edu.cn.

Notes

The authors declare no competing financial interest.

■ ACKNOWLEDGMENTS

We thank the SXRMB beamline of the Canadian Light Source (CLS) and the BL14W1 beamline of the Shanghai Synchrotron Radiation Facility (SSRF) for providing the beam time. This work was supported by the National Basic Research Development Program of China (973 Program, Nos. 2010CB934503, 2011CB808404), the National Natural Science Foundation of China (Nos. 61006015, 51033007, 61274019), the Natural Science Foundation of Jiangsu Province (No. BK2010220), and the Priority Academic Program Development of Jiangsu Higher Education Institutions (PAPD). CLS is supported by NSERC, NRC, CIHR, and University of Saskatchewan. Research at University of Western Ontario is supported by NSERC, CFI, CRC, and OIT.

■ REFERENCES

(1) Kesavan, L.; Tiruvalam, R.; Rahim, M. H. A.; Saiman, M. I. b; Enache, D. I.; Jenkins, R. L.; Dimitrators, N.; Lopez-Sanchez, J. A.; Taylor, S. H.; Knight, D. W.; Kiely, C. J.; Hutchings, G. J. *Science* **2011**, *331*, 195−199.
(2) Chaudhuri, R. G.; Paria, S. *Chem. Rev.* **2012**, *112*, 2373−2433.
(3) Ferrando, R.; Jellinek, J.; Johnston, R. L. *Chem. Rev.* **2008**, *108*, 845−910.
(4) Jiang, H. L.; Xu, Q. *J. Mater. Chem.* **2011**, *21*, 13705−13725.
(5) Zhang, X.; Su, Z. H. *Adv. Mater.* **2012**, *24*, 4574−4577.
(6) Jiang, H. L.; Akita, T.; Ishida, T.; Haruta, M.; Xu, Q. *J. Am. Chem. Soc.* **2011**, *133*, 1304−1306.
(7) Xu, J. G.; Wilson, A. R.; Rathmell, A. R.; Howe, J.; Chi, M. F.; Wiley, B. J. *ACS Nano* **2011**, *5*, 6119−6127.
(8) Tang, S. C.; Vongehr, S.; Meng, X. K. *J. Mater. Chem.* **2010**, *20*, 5436−5445.
(9) Sun, Y. G.; Lei, C. H. *Chem. Int. Ed.* **2009**, *48*, 6824−6827.
(10) Geim, A. K. *Science* **2009**, *324*, 1530−1537.
(11) Weiss, N. O.; Zhou, H. L.; Liao, L.; Liu, Y.; Jiang, S.; Huang, Y.; Duan, X. F. *Adv. Mater.* **2012**, *24*, 5782−5825.
(12) Zhu, Y.; James, D. K.; Tour, J. M. *Adv. Mater.* **2012**, *24*, 4924−4326.
(13) Kamat, P. V. *J. Phys. Chem. Lett.* **2010**, *1*, 520−527.
(14) Huang, X.; Qi, X. Y.; Boey, F.; Zhang, H. *Chem. Soc. Rev.* **2012**, *41*, 666.
(15) Hong, W. J.; Bai, H.; Xu, Y. X.; Yao, Z. Y.; Gu, Z. Z.; Shi, G. Q. *J. Phys. Chem. C* **2010**, *114*, 1822−1826.
(16) Muszynski, R.; Seger, B.; Kamat, P. V. *J. Phys. Chem. L.* **2008**, *112*, 5263−5266.
(17) Shen, J. F.; Shi, M.; Li, N.; Yan, B.; Ma, H. W.; Hu, Y. Z.; Ye, M. X. *Nano Res.* **2010**, *3*, 339−349.
(18) Johnson, J. L.; Behnam, A.; Pearton, S. J.; Ural, A. *Adv. Mater.* **2010**, *22*, 4877−4880.
(19) Wu, C. H.; Wang, C. H.; Lee, M. T.; Chang, J. K. *J. Mater. Chem.* **2012**, *22*, 21466−21471.
(20) Guo, S. J.; Wen, D.; Zhai, Y. M.; Dong, S. J; Wang, E. K. *ACS Nano* **2010**, *4*, 3959−3968.
(21) Yoo, E. J.; Okata, T.; Akita, Y.; Kohyama, M.; Nakamura, J.; Honma, I. *Nano Lett.* **2009**, *9*, 2255−2259.
(22) Rao, C. V.; Cabrera, C. R.; Ishikawa, Y. *J. Phys. Chem. C* **2011**, *115*, 21963−21970.
(23) Guo, S. J.; Dong, S. J.; Wang, E. K. *ACS Nano* **2010**, *4*, 547−555.
(24) Chai, J.; Li, F. H.; Hu, Y. W.; Zhang, Q. X.; Han, D. X.; Niu, L. *J. Mater. Chem.* **2011**, *21*, 17922−17929.
(25) Liu, C. H.; Mao, B. H.; Gao, J.; Zhang, S.; Gao, X.; Liu, Z.; Lee, S. T.; Sun, X. H.; Wang, S. D. *Carbon* **2012**, *50*, 3008−3014.
(26) Torimoto, T.; Okazaki, K.; Kiyama, T.; Hirahara, K.; Tanaka, N.; Kuwabata, S. *Appl. Phys. Lett.* **2006**, *89*, 243117.
(27) Torimoto, T.; Tsuda, T.; Okazaki, K.; Kuwabata, S. *Adv. Mater.* **2010**, *22*, 1196−1221.
(28) Wender, H.; de Oliveira, L. F.; Migowski, P.; Feil, A. F.; Lissner, E.; Prechtl, M. H. G.; Teixeira, S. R.; Dupont, J. *J. Phys. Chem. C* **2010**, *114*, 11764−11768.
(29) Yoshii, K.; Tsuda, T.; Arimura, T.; Imanishi, A.; Torimoto, T.; Kuwabata, S. *RSC Adv.* **2012**, *2*, 8262−8264.
(30) Toshima, N.; Kanemaru, M.; Shiraishi, Y.; Koga, Y. *J. Phys. Chem. B* **2005**, *109*, 16326−16331.
(31) Coulthard, I.; Sham, T. K. *Phys. Rev. Lett.* **1996**, *77*, 4824−4827.
(32) Bzowski, A.; Sham, T. K. *Phys. Rev. B* **1994**, *49*, 13776−13779.
(33) Nahm, T. U.; Jung, R.; Kim, J. Y.; Park, W. G.; Oh, S. J.; Park, J. H.; Allen, J. W.; Chung, S. M.; Lee, Y. S.; Whang, C. N. *Phys. Rev. B* **1998**, *58*, 9817−9825.
(34) Liu, F.; Zhang, P. *Appl. Phys. Lett.* **2010**, *96*, 043105.
(35) Bolin, T.; Wu, T. P.; Schweitzer, N.; Lobo-Lapidus, R.; Kropf, A. J.; Wang, H.; Hu, Y. F.; Miller, J. T.; Heald, S. *Catal. Today* **2013**, *205*, 141−147.
(36) Wu, T. P.; Childers, D. J.; Gomez, C.; Karim, A. M.; Schweitzer, N. M.; Kropf, A. J.; Wang, H.; Bolin, T. B.; Hu, Y. F.; Kovarik, L.; Meyer, R. J.; Miller, J. T. *ACS Catal.* **2012**, *2*, 2433−2443.
(37) Hüfner, S.; Wertheim, G. K.; Wemick, J. H. *Solid State Comm.* **1975**, *17*, 417−422.
(38) Udayabhaskararao, T.; Sun, Y.; Goswami, N.; Pal, S. K.; Balasubramanian, K.; Pradeep, T. *Angew. Chem. Int. Ed.* **2012**, *51*, 2155−2159.
(39) Li, H. Q.; Han, L. N.; Cooper-White, J.; Kim, I. *Green Chem.* **2012**, *14*, 586−591.
(40) Li, J.; Liu, C. Y.; Liu, Y. *J. Mater. Chem.* **2012**, *22*, 8426−8430.

(41) Sibfelt, J. H.; Meitzner, G. D. *Acc. Chem. Res.* **1993**, *26*, 1−6.